Volland, S, Hughes, LC, Kong, C, Burgess, BL, Linberg, KA, Luna, G, Zhou, ZH, Fisher, SK and Williams, DS

Three-dimensional organization of nascent rod outer segment disk membranes

Volland, S. et alt (2015) Three-dimensional organization of nascent rod outer segment disk membranes. *Proceedings of the National Academy of Sciences*, 112 (48). pp. 14870-14875.

doi: 10.1073/pnas.1516309112

Three-dimensional organization of nascent rod outer segment disk membranes

Stefanie Volland[1], Louise C. Hughes[1,5,6 *], Christina Kong[1], Barry L. Burgess[1], Kenneth A. Linberg[7], Gabriel Luna[7], Z. Hong Zhou[3,5,6], Steven K. Fisher[7,8] and David S. Williams[1,2,3,4]

[1]Department of Ophthalmology and Stein Eye Institute, [2]Department of Neurobiology, David Geffen School of Medicine at UCLA, [3]Molecular Biology Institute, [4]Brain Research Institute, [5]Department of Microbiology, Immunology and Molecular Genetics, [6]Electron Imaging Center for Nanoscience, CNSI, University of California, Los Angeles, CA

[7]Neuroscience Research Institute, [8]Molecular, Cellular, and Developmental Biology, University of California, Santa Barbara, CA

* Current address: Department of Biological and Medical Sciences, Oxford Brookes University, Oxford, UK.

Corresponding author:

David S. Williams

Stein Eye Institute, David Geffen School of Medicine at UCLA

100 Stein Plaza, Los Angeles, CA 90095

Email: dswilliams@ucla.edu

Key words: photoreceptor, cilium, EM tomography, disk morphogenesis

Abstract

The vertebrate photoreceptor cell contains an elaborate cilium that includes a stack of phototransductive membrane disks. The disk membranes are continually renewed, but how new disks are formed remains poorly understood. Here, we used electron microscope tomography to obtain 3-D visualization of the nascent disks of rod photoreceptors in three mammalian species, in order to gain insight into the process of disk morphogenesis. We observed that nascent disks are invariably continuous with the ciliary plasma membrane, although, due to partial enclosure, they can appear to be internal in 2-D profiles. Tomographic analyses of the basal-most region of the outer segment show changes in shape of the ciliary plasma membrane indicating an invagination, which is likely a first step in disk formation. The invagination flattens to create the proximal surface of an evaginating lamella, as well as membrane protrusions that extend between adjacent lamellae, thus initiating a disk rim. Immediately distal to this initiation site, lamellae of increasing diameter were evident, indicating growth outward from the cilium. In agreement with a previous model, our data indicate that mature disks are formed once lamellae reach full diameter, and the growth of a rim encloses the space between adjacent surfaces of two lamellae. The present study provides 3-D data of nascent and mature rod photoreceptor disk membranes at unprecedented z-axis depth and resolution, and provides a basis for addressing fundamental questions that range from protein sorting in the photoreceptor cilium to photoreceptor electrophysiology.

Significance

A vertebrate photoreceptor cell depends upon the elaboration of its cilium to generate its light-sensitive organelle, the outer segment (OS), which is made up of a stack of membrane disks, containing the visual receptor, opsin. How this elaboration occurs has been the subject of recent controversy. Here, we have used electron microscope tomography to obtain a 3-D analysis of the membrane organization at the base of the OS, where new membrane disks are continually made to replace the older ones. We show that the nascent disk membrane is continuous with the ciliary plasma membrane, and appears to form by a complex reshaping of this membrane, involving an invagination, followed by outward growth, and, finally, the completion of a disk rim.

Introduction

\body

Primary cilia detect extracellular signals via membrane receptors or channels. The most elaborate of all cilia, the cilium that forms the vertebrate photoreceptor outer segment (OS), includes a large stack of membrane disks that extends distally from the transition zone, also known as the connecting cilium (1). The OS disks contain the visual receptor, opsin, and their tight packing allows for a high concentration of opsin within a confined space, thus limiting the trade-off between visual sensitivity and spatial resolution. Turnover of OS disk membranes occurs throughout the lifetime of an animal (2), and requires the *de novo* synthesis and degradation of large amounts of OS proteins; on average, 9-10 billion opsin molecules are turned over every second in each human retina (3).

A key event in OS disk turnover is the formation of disk membranes from newly synthesized molecules that are trafficked as vesicles from the ER/Golgi in the inner segment to the cilium (4, 5). Disk membrane morphogenesis is essential for the survival of photoreceptor cells. Orthologs of gene mutations that disrupt disk formation in mice have been linked to a variety of retinal degenerations in humans. For examples, in the *rds* mouse (mutant in *Prph2*), disks do not develop from the end of the connecting cilium (6, 7), and in mice whose photoreceptors express mutant human *PROML1*, the disks that do form are disorganized (8). *PRPH2* and *PROM1* genes have been linked to different forms of retinitis pigmentosa, macular dystrophy, and cone-rod dystrophy (https://sph.uth.edu/retnet/disease.htm).

Disk membrane morphogenesis clearly involves extensive membrane growth and shaping, however the process by which these events occur remains largely unresolved. Although there is agreement that mature rod OS disks appear discrete and enclosed entirely by the plasma membrane, models differ fundamentally according to whether the nascent disks form from the ciliary plasma membrane or from the expansion of endosomal

membrane. Differences stem from interpretation of whether the nascent disks are open to the extracellular space (9, 10), or closed from it, like the mature disks (11). Whether the nascent disks are open or closed also has important implications for understanding questions of photoreceptor cell biology and electrophysiology, such as how membrane proteins are sorted into the subdomains of the OS (12) and the origin of the early receptor potential (13).

There are several possible reasons for the different interpretations of whether nascent rod disks are open or closed, including differences in method of tissue preservation, species differences, and perhaps differences in the time of day when the retinas were fixed. In an attempt to resolve the discrepancy, we have addressed these variables in the present study. Importantly, we have also addressed a limitation of the previous studies, the reliance on 2-D conventional TEM, by using TEM tomography (ET) to generate the first substantial high-resolution 3-D reconstruction of the nascent disks of single rod photoreceptor cells. Our 3-D analysis illustrates that nascent disks consistently possess continuities with the ciliary plasma membrane, thus supporting a model in which their morphogenesis occurs by amplification of this membrane. However, our analysis also demonstrates a previously unappreciated feature of nascent disk organization, and provides novel insight into the first stages of disk morphogenesis.

Results

Preservation of disk membranes

Mouse photoreceptor OSs are notoriously difficult to preserve well for TEM, perhaps due in part to their very high packing density, which, for most of the retina, is 3-4 times greater than the photoreceptor density in the human macula (14), and may impede the penetration of fixative. Nascent disk membranes may be especially labile, given their transient state, so that variations in the quality of preservation may be responsible for differing reports on whether the nascent disks in mouse rods are open (15) or closed (16, 17).

Cardiac perfusion with Karnovsky's fixative resulted in OS disk membranes that were well organized (Fig. 1A) – significantly better than when an opened eyecup was simply immersed in the same fixative. Mitochondria (a sensitive indicator of fixation quality) were also well-preserved in the apical inner segment. In addition, we tested the use of high-pressure freezing, followed by freeze substitution (HPF-FS). However, because the retina is not immediately accessible, HPF-FS could only be performed following dissection of the eye and preparation of small retinal pieces. To avoid artifacts that might occur during dissection, we preceded it with a brief period of cardiac perfusion with Karnovsky's fixative. Previous reports have shown that aldehyde fixation prior to HPF-FS provides results similar to the preservation by HPF-FS alone (18). This approach generated well-preserved photoreceptor ultrastructure, with disk membranes that presented linear, parallel profiles (Fig. 1B).

Fixation by cardiac perfusion of larger mammals resulted in high-quality preservation of OS disks and the photoreceptor mitochondria (Fig. 1C-E). Notably, we were able to observe basal nascent disks that were continuous with the plasma membrane, regardless of species (arrows in Fig. 1A-D).

ET of nascent disk membranes

ET was performed on 300-nm sections. A video of a tomogram of the basal OS of a mouse rod, preserved by HPF-FS, and a 3-D model from this tomogram are shown in Suppl. 1 and 2. In some cases, to increase z-axis depth so that it included most of the rod OS diameter, tomograms from serial 300-nm sections were joined along the z-axis. From the resulting large tomogram, we observed some z-plane images of rod OSs from mouse, cat and monkey retinas, in which the basal disks appeared closed (e.g. Fig. 2A, E). Invariably, however, these basal disks were observed to be continuous with the plasma membrane in other z-planes; that is, the disks possessed an opening to the extracellular space. This is demonstrated in Fig. 2A-C, showing four basal-most “disks” of a monkey rod in different z-planes. In the z-plane illustrated in Fig. 2A, the red arrow indicates the four appearing as isolated internal structures, however, note that indentations of the plasma membrane occurs opposite each of these. In the plane shown in Fig. 2B, both the internal “disks” and the indentations of the plasma membrane have grown longer (blue arrow), and in the z-plane shown in Fig. 2C, they are joined, so that the “disks” are continuous with the plasma membrane, showing that they are actually lamellae (yellow arrow). Suppl. 3 contains a video of four consecutive tomograms of these disks. A 3-D model obtained from segmentation is shown in Fig 2D.

In another example, images from three z-planes of a cat rod photoreceptor are shown in Figs. 2E-G. Three nascent disks are shown, one of which appears as little more than an elongated vesicle (red arrow). However, following this “vesicle” through different z-planes of the tomogram (also Suppl. 4), reveals that it is continuous with the plasma membrane (yellow arrow, Fig. 2G). The resulting model from segmentation of the tomogram illustrates the 3-D structure of this membrane structure and its connection to the plasma membrane; it represents a slightly flattened tubule that may have resulted from an invagination of the plasma membrane (arrows in Fig. 2H).

Nascent disk initiation

Analyses of the basal-most folding of the plasma membrane in tomograms from cat, mouse, and monkey rod OSs show a variety of structures similar to that illustrated in Fig. 2H. An example is shown from a tomogram of a monkey rod (Fig. 3A-C). The model created by segmentation of that tomogram (Fig. 3D-E, Suppl. 5) shows one of these structures that appears bi-lobed (arrows, Fig. 3D). Since these are always the basal-most structure associated with disk formation, they invariably occur in a thickened area of the connecting cilium, and they can manifest various degrees of lateral expansion from their most inner region.

These observations suggest that disk morphogenesis may be initiated by an invagination of the plasma membrane that helps shape a membrane lamella, and contributes to the initiation of disk rim formation as the invagination expands laterally. Distal to this initiation structure, the membrane appears as a series of lamellae, with the more distal lamellae extending further outward (e.g. Fig. 3A), indicating the presence of outward growth, or an evagination process (which can be rather uneven, as illustrated in Fig 2A-D).

Closure of the nascent disks (lamellae) by rim completion

Steinberg et al. (10) proposed that the basal lamellae become internalized as the disk rim is completed around the space between two adjacent lamellae. Analyses of our tomograms support this view, as illustrated in the example of selected z-planes and 3-D modeling of a tomogram of a mouse rod, as shown in Fig. 3F-J and Suppl. 6. In Fig. 3F, the 12 basal-most “disks” appear more dilated than the mature distal disks, a characteristic described previously for the basal lamellae in frog rod photoreceptors (19). In this z-plane, the three “disks” above the red arrow appear to be enclosed by the plasma membrane, but still show the dilated morphology, while the other 9 “disks” (red arrow and below) appear open. In a different z-plane, the fourth most distal “disk” appears enclosed (yellow arrow, Fig. 3H). In a

z-plane intermediate to those shown in Figs. 3F and 3H, the tip of this fourth “disk” appears to be in contact with the enveloping plasma membrane (blue arrow, Fig. 3G). In a 3-D model created from segmentation of this tomogram (Fig. 3I), the point of contact can be seen as a transition zone between an area that is open (above the lamella indicated by the red arrow, and to the left of the blue arrow) and an area that is enclosed by the plasma membrane (to the right of the blue arrow). The blue arrow indicates what appears to be the leading edge of a disk rim forming from right to left. The dilated appearance of disks enclosed in a single z-plane by the plasma membrane suggests that these are indeed not mature disks but represent lamellar outgrowths that are transitioning into mature disks, i.e. the process of rim formation and plasma membrane growth is incomplete leaving a small opening to the extracellular space.

Calycal process of mouse rod photoreceptor

Calycal processes arising from the inner segment and surrounding the base of the OS are a generally accepted feature of photoreceptors in most vertebrates, although recently it was claimed that they are absent in mouse (20). Tomographic data from the base of mouse rod OSs revealed that they indeed possess a single, tongue-like calycal process, opposite the connecting cilium. This process is evident as an extension from the inner segment to the right of the nascent and more distal disks in the single z-planes shown in Fig. 3F-H, and in the 3-D visualizations of segmented tomograms (Fig. 3I, J; Suppl. 7).

Nascent disks on a daily cycle

The rate of addition of new disks to frog rod OSs varied greatly according to a daily cycle, with the number of open discs increasing three-fold during the first 8 h of light in comparison to the dark portion of the L/D cycle (21). Such cyclic variation may also help explain the controversy surrounding open and closed nascent disks in mammals. Thus, we recorded the

number of basal lamellae (open nascent disks) in monkey and mouse rods at different times of day. While lamellae were evident at all times sampled in both species, the number increased during the first part of the light period in monkey, similar to that reported for frog rods (21), but decreased during the same period in mouse rods (Fig. 4), suggesting a possible relationship between the diurnal and nocturnal habits of monkey and mouse, respectively.

Discussion

By ET of rod photoreceptor nascent disks from different species and using various fixation techniques, we have been able to address issues of disk membrane formation in a way not approached in earlier studies. The tomographic data not only allowed us to create very high-resolution z-axis images (3-4 nm) of the nascent disk-forming region, but also to create high-resolution 3-D models from the data. Previous studies, which typically relied on 2-D images of ~70-nm sections, have reported conflicting interpretations of nascent disk organization and hence mature disk formation. Our analyses by ET of 300-nm sections showed that the nascent disks are continuous with the ciliary plasma membrane (thereby classified as lamellae), and appeared to form by expansion of the plasma membrane. Our results also indicated novel information with regard to disk initiation.

Early TEM studies of mammalian retinas observed that the disk membranes of cone photoreceptors and the basal disk membranes of rod photoreceptors are continuous with the ciliary plasma membrane (22-24). These observations led to the hypothesis that new disks are formed by invaginations of the ciliary plasma membrane (9). Steinberg et al. (10) also reported the nascent OS disks to be continuous with the ciliary plasma membrane, but concluded that the growth of the disk membranes occurs by an evagination rather than an invagination. Importantly, this study also proposed the formation of the disk rim as the final growth stage. Studies of frog photoreceptors not only found that the nascent disks are amplifications of the plasma membrane (19), but, using Lucifer yellow as an extracellular tracer, they were able to label the nascent disks, thus demonstrating that they are open to the extracellular space (25).

Relatively recently, Sung and colleagues reported observing the nascent disks of mouse rods to be completely internal, and proposed models of disk morphogenesis in which the disks form by expansion of vesicular membrane (11, 16). They argued that data for the earlier, open disk models came from tissue that was inadequately fixed, and postulated that

the use of a mixture of formaldehyde and acrolein preserves disk membranes closer to their native state. However, while acrolein, a monoaldehyde introduced for TEM by Luft (26), has an advantage of rapid tissue penetration, its use has been limited because of reports that it solubilizes membranes (27). In addition, the notion that ordered membrane lamellae would form as artifacts from vesicles seems unlikely. It is noteworthy that, in images of the HPF-FS samples (Fig. 1B) and also some of the conventionally-processed samples (e.g. Fig. 1A and D), the surfaces of neighboring lamellae appear very close to each other, with a spacing that resembles the intradiskal space of the mature disks, measured to be ~4 nm (28). This observation indicates that the growing lamellae already possess a highly-ordered characteristic of the mature disk membranes. Moreover, the proximity of the adjacent lamellar surfaces may be sufficient to result in a force that drives the smaller lamella outward, following its more mature, distal neighbor (29).

It has been noted that species difference may play a role in the controversy because the rate of disk formation varies by species (30). However, there are different studies that all used mouse retinas, but reported both open (15), and closed (16, 17, 31) disks, suggesting that species difference alone does not provide a satisfactory explanation for the various observations. Nevertheless, in order to address the possibility of different results related to different methods of fixation and species, we tested three different mammalian species, as well as different methods for the preservation of mouse photoreceptors, including the use of HPF-FS.

Rapid freezing of cells provides a much faster preservation than chemical fixation. HPF is particularly advantageous for tissues, since it suppresses ice crystal formation, and, compared with freezing at ambient pressure, permits the freezing of much larger samples, (32, 33). A recent study on the ultrastructure of the cilium and striated rootlet of mouse rods by cryo-ET used plunge-freezing of a purified OS suspension (31). Although this study provided novel ultrastructural detail, tomograms were limited to very small z-axis depth,

which compromised the extent of 3-D segmentation. When combined with FS, HPF results in material that can withstand the extensive high-voltage exposure that is necessary for the substantial z-axis imaging for ET (34). Yet, even the amount of tissue that can be preserved by HPF is quite limited (up to 0.2-0.5 mm thick), necessitating prior dissection, during which cells can become damaged. Here, in order to stabilize the retina prior to dissection for HPF-FS, we used a brief cardiac perfusion with Karnovsky's fixative. This approach has been demonstrated with accessible cells, such as those in cell culture, to generate tissue preservation that is close to that by HPF-FS alone (18). Chemical fixation, followed by HPF-FS is considered superior to conventional aldehyde fixation methods because it avoids the subsequent ambient temperature processing steps (18), during which lipids may be extracted (35). This conclusion is consistent with the linear, parallel profiles that we obtained of mouse OS disks prepared by HPF-FS, but not by chemical fixation alone (cf. Fig. 1B with 1A). Importantly, however, we did not observe any difference, with respect to whether nascent disks were open or closed, between rod OSs that were fixed and processed by HPF-FS and those fixed by perfusion with Karnovsky's fixative and processed by conventional TEM methods.

Our results with the three different mammalian species are largely consistent with the model of disk morphogenesis proposed by Steinberg et al. (10). In this model, nascent disks are continuous with the ciliary plasma membrane, at least at some region around their perimeter. Their increase in width associated with a more distal position is consistent with growth out from the axoneme; i.e. growth by evagination. A significant difference in our data is reflected by the greater detail we were able to obtain of membrane organization at the most basal part of the disk stack by ET. Here, *invaginations* of varied shapes appear in a bulge of the ciliary plasma membrane, suggesting that the initiation of a new lamella begins with a bulge and then an invagination of the ciliary plasma membrane. We propose that this invagination is important for generating the flattened organization of a lamella, and the

lateral expansion of the innermost surface of the invagination (closest to the axoneme) initiates the circumferential processes that becomes the disk rim (Fig. 5A, B). Subsequent outward growth of the lamella (Fig. 5C) is followed by completion of the disk rim (Fig. 5D), and resulting enclosure of the space between the lamellae to create a mature disk completely enclosed by the plasma membrane (Fig. 5E). A mature disk is thus formed from the adjacent membranes of two lamellae, and contains what was originally extracellular space (Fig. 5); as noted above, the very small space between two adjacent lamellae appears similar to that between the two membranes of a mature disk. It has been shown that the initiation of new disks, but not the growth of the evaginations, requires f-actin (36, 37), so that the membrane invagination, a critical first step in the process, may be dependent on an actin mechanism.

Whether the nascent disks are open or closed is also important with respect to other aspects of photoreceptor cell biology and electrophysiology. As the disk membranes are formed, critical sorting or at least maintenance of a separation of membrane proteins must occur. Within the disk membranes themselves, rim proteins (e.g. PRPH2, ROM1, ABCA4) are separated from proteins that will occupy the disk surfaces (e.g. RHO). In addition, proteins that function in the plasma membrane (e.g. the cGMP channel subunit proteins, such as CNGA1) must be separated from discrete disk membranes (12). ImmunoEM and trafficking studies of PRPH2 show that this protein is delivered to the cilium separately from RHO (38), and that it is not included in the most basal disks of rod OS (36, 39), consistent with an open lamellar structure for the basal disks. The presence of PRPH2 in the OS coincides only with rim formation (39, 40). CNGA1 appears to be trafficked directly to the rod OS plasma membrane, distal to the nascent disk region (36).

The early receptor potential (ERP), first reported by Brown and Murakami (41), appears to be generated by the movement of charge within each rhodopsin molecule as it changes its conformation upon photobleaching. However, because the ERP occurs across

the plasma membrane, only rhodopsin molecules that are in the plasma membrane can contribute to it. The signal from mammalian rods is too large to be explained without a subset of disks being open to the extracellular space, and thus increasing the effective rhodopsin content of the plasma membrane (13). If the nascent disks are open, they could contribute to the ERP; if not, some of the mature rod disks must be exposed to the extracellular space, an observation not made in any studies to date.

The focus of this study has been on the organization of the nascent disks of rod photoreceptors. An additional observation made during the study deserves comment because of a recent report that mouse photoreceptors do not possess calycal processes (20). In our z-stack of images from the tomograms of mouse OSs, we were able to identify the presence of a calycal process, opposite the connecting cilium. A similar, single calycal process has been shown in rat rod photoreceptors (39, 42).

Material and Methods

Animals and sample preparation. C57BL/6J mice were housed at UCLA and used at 6 weeks old. Cats, *Felis catus*, and rhesus monkeys, *Macaca mulatta*, were housed at UCSB, and used as adults. All animals were kept on a 12 h light/12 h dark cycle, and treated in accordance with appropriate institutional guidelines. Mouse retinas were fixed by immersion of posterior eyecups in 2% formaldehyde, 2.5% glutaraldehyde in 0.1 M phosphate buffer, or by transcardiac perfusion for 30 min with the same fixative. For conventional TEM, eyecups were postfixed in 1% OsO_4 in 0.1 M cacodylate buffer for 1 h, dehydrated, and embedded in Araldite 502. Retinal tissue for HPF-FS was dissected after 5 min of cardiac perfusion with 50 mL of fixative, and small pieces (approx. 1 mm x 1 mm x 0.2 mm) were placed in specimen carriers, transferred to a sample holder and frozen in a Leica EMpact2 high-pressure freezer (Leica). Samples were then placed in cryo-substitution medium, containing 1% OsO_4 and 0.1% uranyl acetate in acetone, within an automatic freeze substitution unit EMafs2 (Leica). The temperature was raised slowly for 88 h to room temperature, while the fixative gradually replaced the water in the sample. Samples were then washed in acetone and propylene oxide, and embedded in Araldite 502. Cat and monkey tissue was fixed using transcardiac perfusion, as described previously (43, 44). For conventional TEM, ~70-nm sections were stained with 5% uranyl acetate and 0.4% lead citrate. Serial sections of 300-nm thickness were collected for ET on formvar-coated, copper slot grids, and stained with 10% uranyl acetate in methanol and 0.4% lead citrate. Additionally, sections were labeled with 15- and 20-nm colloidal gold fiducials on the top and the bottom of each grid, respectively, to aid in the alignment of images in each tilt series.

ET Methods. ET was performed with an FEI Technai TF20, operated at 200kV. Images were recorded using a 16-megapixel CCD camera (TVIPS) at original magnifications between 14,500x and 19,000x. Serial sections were imaged using double tilt axis

tomography with the “Batch Tomography” software from FEI. The series were recorded with an underfocus of approx. -5 µm from -70° to +70° along two tilt axes, with 2° increments at the lower tilt angles (range ±40°) and 1° increments above +40° and below - 40°. To obtain the dual tilt data sets, the grid was rotated by 90° after the acquisition of a single tilt axis, and a second tilt series was recorded in the same location.

Data Processing. The images acquired in each tomography tilt series were aligned and combined to generate a tomographic reconstruction of the imaged 300-nm section using “eTomo” (IMOD, Boulder, CO). Fiducial-based alignment was used. After separate tomographic reconstructions were generated, tomograms from serial sections were joined into one volume along the z-axis, using a function of eTomo, “Join Serial Tomograms”, which runs a series of programs, including and the interactive program, *MIDAS*, for alignment, as well as programs for joining. Segmentation and subsequent image processing were conducted using “3dmod” (http://bio3d.colorado.edu/imod/). In tomograms acquired from monkey and mouse, the membrane structures at the base of the rod OS were traced in every 3 to 10 z-slices to create a 3-D model. Different regions of the photoreceptor were modeled as separate, enclosed objects. The OS plasma membrane, disk lamellae, and ciliary plasma membrane were modeled as one object, while the inner segment plasma membrane was modeled as another object, even though all these membranes are continuous. Segmentation and subsequent image processing of cat tomograms were conducted using Amira (Version 5.2.0, FEI, Hillsboro, OR). Segmentation was based upon distinct characteristics of the data; regions of interest (ROI) were selected, and data within the ROI were displayed using the functions "thresholding" and "smoothing". Different colors display separate membrane compartments. Videos of 3-D models were generated using the interactive visualization program Chimera (UCSF, San Francisco, CA), while videos of tilt

series and tomogram reconstructions were generated using 3dmod (IMOD, Boulder, CO) and Fiji (NIH), an open source processing package based on ImageJ.

Open disk quantification. To obtain the number of open disks at multiple time points throughout the day, electron micrographs of well-aligned rod outer segments that included a longitudinal section of the axoneme were taken from mouse and monkey retinas that had been prepared for conventional TEM. The number of observable open disks were counted on the side opposite the axoneme in 15-28 rod photoreceptors from several sections from one animal for each time of day. Statistical analyses to test for variation among different times of day were performed using ANOVA.

Acknowledgments

We greatly appreciate the advice and help provided by Xinran Liu (Yale University) at the start of this project, and the valuable discussions on membrane properties with Wayne Hubbell (UCLA) and Jacob Israelachvili (UCSB). The work was supported by grants from the NIH (EY013408, EY024667, EY000331, GM071940). We acknowledge use of instruments at the Electron Imaging Center for Nanomachines, supported by UCLA and by an instrumentation grant from the NIH (S10RR23057).

References

1. Besharse JC & Horst CJ (1990) The photoreceptor connecting cilium: a model for the transition zone. *Ciliary and flagellar membranes*, ed Bloodgood RA (Plenum Press, New York), pp 409-431.
2. Young RW (1967) The renewal of photoreceptor cell outer segments *J. Cell Biol.* 33:61-72.
3. Williams DS (2002) Transport to the photoreceptor outer segment by myosin VIIa and kinesin II *Vision Res.* 42:455-462.
4. Papermaster DS, Schneider BG, & Besharse JC (1985) Vesicular transport of newly synthesized opsin from the Golgi apparatus toward the rod outer segment. Ultrastructural immunocytochemical and autoradiographic evidence in Xenopus retinas *Invest. Ophthalmol. Vis. Sci.* 26:1386-1404.
5. Deretic D & Papermaster DS (1991) Polarized sorting of rhodopsin on post-Golgi membranes in frog retinal photoreceptor cells *J. Cell Biol.* 113:1281-1293.
6. Sanyal S & Jansen HG (1981) Absence of receptor outer segments in the retina of rds mutant mice *Neurosci. Lett.* 21:23-26.
7. Cohen AI (1983) Some cytological and initial biochemical observations on photoreceptors in retinas of rds mice *Invest. Ophthalmol. Vis. Sci.* 24:832-843.
8. Yang Z*, et al.* (2008) Mutant prominin 1 found in patients with macular degeneration disrupts photoreceptor disk morphogenesis in mice *J. Clin. Invest.* 118:2908-2916.
9. Nilsson SE (1964) Receptor Cell Outer Segment Development and Ultrastructure of the Disk Membranes in the Retina of the Tadpole (Rana Pipiens) *J. Ultrastruct. Res.* 11:581-602.
10. Steinberg RH, Fisher SK, & Anderson DH (1980) Disc morphogenesis in vertebrate photoreceptors *J. Comp. Neurol.* 190:501-508.
11. Sung CH & Chuang JZ (2010) The cell biology of vision *The Journal of cell biology* 190:953-963.
12. Molday RS & Molday LL (1987) Difference in the protein composition of bovine retinal rod outer segment disk and plasma membrane isolated by a ricin-gold-dextran density perturbation method *J. Cell Biol.* 105:2589-2601.
13. Woodruff ML, Lem J, & Fain GL (2004) Early receptor current of wild-type and transducin knockout mice: photosensitivity and light-induced Ca2+ release *J. Physiol.* 557:821-828.
14. Volland S, Esteve-Rudd J, Hoo J, Yee C, & Williams DS (2015) A comparison of some organizational characteristics of the mouse central retina and the human macula *PLoS One* 10:e0125631.
15. Carter-Dawson LD & LaVail MM (1979) Rods and cones in the mouse retina. I. Structural analysis using light and electron microscopy *J. Comp. Neurol.* 188:245-262.
16. Chuang JZ, Zhao Y, & Sung CH (2007) SARA-regulated vesicular targeting underlies formation of the light-sensing organelle in mammalian rods *Cell* 130:535-547.
17. Chakraborty D, Conley SM, Al-Ubaidi MR, & Naash MI (2014) Initiation of Rod Outer Segment Disc Formation Requires RDS *PLoS One* 9:e98939.
18. Sosinsky GE*, et al.* (2008) The combination of chemical fixation procedures with high pressure freezing and freeze substitution preserves highly labile tissue ultrastructure for electron tomography applications *J. Struct. Biol.* 161:359-371.
19. Besharse JC, Hollyfield JG, & Rayborn ME (1977) Turnover of rod photoreceptor outer segments. II. Membrane addition and loss in relationship to light *The Journal of cell biology* 75:507-527.

20. Sahly I*, et al.* (2012) Localization of Usher 1 proteins to the photoreceptor calyceal processes, which are absent from mice *The Journal of cell biology* 199:381-399.
21. Besharse JC, Hollyfield JG, & Rayborn ME (1977) Photoreceptor outer segments: accelerated membrane renewal in rods after exposure to light *Science* 196:536-538.
22. Sjöstrand FS (1959) The organization of membrane layers *Rev Mod Phys* 31:301-318.
23. Moody MF & Robertson JD (1960) The fine structure of some retinal photoreceptors *J Biophys Biochem Cytol* 7:87-92.
24. Dowling JE (1967) The organization of vertebrate visual receptors. *Molecular organization and biological function*, ed Allen JM (Harper & Row, New York).
25. Matsumoto B & Besharse JC (1985) Light and temperature modulated staining of the rod outer segment distal tips with Lucifer yellow *Invest. Ophthalmol. Vis. Sci.* 26:628-635.
26. Luft JH (1959) The use of acrolein as a fixative for light and electron microscopy *Anat Record* 133:305.
27. Glauert AM (1975) *Fixation, dehydration and embedding of biological specimens* (Elsevier, North Holland, New York) Fixation, dehydration and embedding of biological specimens.
28. Nickell S, Park PS, Baumeister W, & Palczewski K (2007) Three-dimensional architecture of murine rod outer segments determined by cryoelectron tomography *J. Cell Biol.* 177:917-925.
29. Israelachvili JN (2011) *Intermolecular and Surface Forces* (Academic Press, Oxford, UK) 3rd Ed.
30. Pearring JN, Salinas RY, Baker SA, & Arshavsky VY (2013) Protein sorting, targeting and trafficking in photoreceptor cells *Prog. Retin. Eye Res.* 36:24-51.
31. Gilliam JC*, et al.* (2012) Three-dimensional architecture of the rod sensory cilium and its disruption in retinal neurodegeneration *Cell* 151:1029-1041.
32. Dahl R & Staehelin LA (1989) High-pressure freezing for the preservation of biological structure: theory and practice *J. Electron Microsc. Tech.* 13:165-174.
33. Studer D, Graber W, Al-Amoudi A, & Eggli P (2001) A new approach for cryofixation by high-pressure freezing *J. Microsc.* 203:285-294.
34. McDonald KL & Auer M (2006) High-pressure freezing, cellular tomography, and structural cell biology *Biotechniques* 41:137-143.
35. Korn ED & Weisman RA (1966) I. Loss of lipids during preparation of amoebae for electron microscopy *Biochim. Biophys. Acta* 116:309-316.
36. Nemet I, Tian G, & Imanishi Y (2014) Submembrane assembly and renewal of rod photoreceptor cGMP-gated channel: insight into the actin-dependent process of outer segment morphogenesis *J. Neurosci.* 34:8164-8174.
37. Williams DS, Linberg KA, Vaughan DK, Fariss RN, & Fisher SK (1988) Disruption of microfilament organization and deregulation of disk membrane morphogenesis by cytochalasin D in rod and cone photoreceptors *J. Comp. Neurol.* 272:161-176.
38. Tian G*, et al.* (2014) An unconventional secretory pathway mediates the cilia targeting of peripherin/rds *J. Neurosci.* 34:992-1006.
39. Arikawa K, Molday LL, Molday RS, & Williams DS (1992) Localization of peripherin/rds in the disk membranes of cone and rod photoreceptors: relationship to disk membrane morphogenesis and retinal degeneration *J. Cell Biol.* 116:659-667.
40. Molday RS, Hicks D, & Molday L (1987) Peripherin. A rim-specific membrane protein of rod outer segment discs *Invest. Ophthalmol. Vis. Sci.* 28:50-61.
41. Brown KT & Murakami M (1964) A New Receptor Potential of the Monkey Retina with No Detectable Latency *Nature* 201:626-628.
42. Kessel RG & Kardon RH (1979) Nervous tissue - eye and ear. *A text atlas of scanning electron microscopy*, ed Kessel RG (W.H. Freeman, San Francisco).

43. Anderson DH & Fisher SK (1979) The relationship of primate foveal cones to the pigment epithelium *J. Ultrastruct. Res.* 67:23-32.
44. Fisher SK & Steinberg RH (1982) Origin and organization of pigment epithelial apical projections to cones in cat retina *J. Comp. Neurol.* 206:131-145.

Figure Legends

Fig. 1. Fixation of disk membrane morphology. (*A*-*B*) TEMs of the basal disks of mouse rod OSs, preserved by transcardiac perfusion with Karnovsky's fixative and conventional processing (*A*), or by brief transcardiac perfusion with Karnovsky's fixative, followed by HPF-FS (*B*). (*C, D*) TEMs of the basal disks of monkey (*C*) and cat (*D*) rod OSs, preserved by transcardiac perfusion with Karnovsky's fixative and conventional processing. In *A*-*D*, the most basal "disks" appear to be open to the extracellular space (and are thus lamellae); indicated by arrows. (*E*) A typical elongated, well-preserved mitochondrion from the inner segment (adjacent to the basal OS disks) from a cat rod. Scale bar, 500 nm; *A*-*E* are at the same magnification. *B* and *C* are z-slices from tomograms; other panels are from TEMs of 70-nm sections.

Fig. 2. Continuity of nascent disks with the plasma membrane. (*A*-*D*) monkey, (*E*-*H*) cat. (*A*-*C, E*-*G*) Different z-plane images from tomograms of the basal disks of rod OSs. Basal disks appear enclosed in one plane of section (red arrow in *A* and *E*), but are actually open to the extracellular space in another plane of section (yellow arrows in *C* and *G*). (*D*, *H*) 3-D renderings of the membrane structures. The arrows (red, blue and yellow) indicate corresponding areas in the z-plane images (*A*-*C*, *E*-*G*) and the respective 3-D models (*D*, *H*). Scale bars, 250 nm (*A*), 100 nm (*D*). *A*-*C*, *E*-*G* are at the same magnification, as are *D* and *H*.

Fig. 3. EM tomography of nascent disk initiation and rim formation. (*A*-*E*) monkey, (*F*-*J*) mouse. (*A*-*C*) Different z-plane images from a tomogram of monkey rod OS basal disks show different profiles of a membrane structure (red, blue and yellow arrows) that in 3-D renderings appears as a bi-lobed invagination (*D* and *E*). *E* is from Suppl. 5; plasma

membrane is green, mature disks are dark blue. (*F-H*) Different z-plane images from a tomogram of mouse rod OS basal disks. Arrows indicate the location of rim formation, so that below the arrows the nascent disks appear as lamellae, and above them they appear enclosed by the plasma membrane. (*I*) 3-D rendering depicts a view from outside the cell: the space above the most mature lamella (red arrow) is partially closed (to the right of the blue arrow); to the left of the blue arrow this space is still open. (*J*) Lower magnification of the 3-D model. The inner segment and a calycal process (light blue) have been modeled separately from other plasma membrane (green). *J* is a frame of the video in Suppl. 7. Scale bars, 250 nm (*A*), 50 nm (*D*), 500 nm (*E*). *A-C*, *F-H* are at the same magnification, as are *D* and *I*, and *E* and *J*.

Fig. 4. Number of open disks throughout the daily cycle. Graph of the number of open disks counted at different times of day at the base of monkey and mouse rod OSs. Error bars indicate $\pm$SD. The probability of no significant difference among the different times of day was determined by ANOVA statistical tests to be < 0.001 for each species.

Fig. 5. Diagram of the organization of the nascent disks of a rod outer segment. Horizontal sections at different locations of the vertical section are shown in *A-E*. (*A*) An invagination that appears to initiate flattening of a protrusion of the ciliary plasma membrane. (*B*) Lateral expansion of the invagination (arrows in *A*) leads to the beginning of rim growth (arrows in *B*). (*C*) Lamella growth outwards. (*D*) Growth of the rim leads to the enclosure of extracellular space between two adjacent lamellae, and thus the formation of a mature disk, which is discrete from the plasma membrane (*E*).

Supplement

Supplement 1. Video showing a double-tilt tomogram of the basal area of a mouse rod OS fixed by brief cardiac perfusion followed by HPF-FS. The video progresses from the photoreceptor periphery towards the central area. Two distinct nascent disks that are open (and are therefore lamellae) are revealed at the OS base. The surfaces of the lamellae appear very close to each other, with a spacing that resembles the intradiskal space of the mature disks, which are above and enclosed by the OS plasma membrane. Z-slices were exported from 3dmod as a tiff file and then converted into a video using Fiji. An individual image of one of the z-slices is shown in Fig. 1B.

Supplement 2. Video showing the 3-D model of a tomogram of a mouse rod OS fixed by brief cardiac perfusion followed by HPF-FS. The video shows the plasma membrane and nascent disks modeled in green and the mature disks modeled in dark blue. The 3-D model rotates and then zooms in, showing the ends of 2 nascent disks (lamellae). This 3-D model is based on segmentation of the tomogram shown in Suppl. 1. The video has been made using Chimera.

Supplement 3. Video showing 4 joined serial, double-tilt tomograms of the basal area of a monkey rod OS. The video includes approximately two thirds of the OS diameter, from the periphery to beyond the central area where the axoneme is visible. The region of interest appears in the center. Every second z-slice was exported from 3dmod as a tiff file and then converted into a video using Fiji. Images of individual z-slices are shown in Fig. 2*A*-*C* and Fig. 3*A*-*C*.

Supplement 4. Video showing a double-tilt tomogram of the basal area of a cat rod OS. The video passes through the OS from the central region where the axoneme is evident to the periphery. A small membranous structure at the base of the ROS appears to be enclosed in the central area of the photoreceptor, but this structure can be traced as the video passes through different z-planes, and in the final frames, it is evident that the structure is continuous with the plasma membrane, thus representing an invagination that is open to the extracellular space. Every z-slice was exported from 3dmod as a tiff file and then converted into a video using Fiji. Images of individual z-slices are shown in Fig. 2*E*-*G*, and a view of 3-D segmentation is in Fig. 2*H*.

Supplement 5. Video showing a 3-D model of two joined serial tomograms of a monkey rod OS. The video shows the plasma membrane modeled in green and the mature disks modeled in dark blue. The plasma membrane includes the ciliary plasma membrane, the membrane enclosing the mature disks, and the nascent disks, which are mostly lamellae, open to the extracellular space. The 3-D model rotates and then zooms in on a bi-lobed invagination at the OS base (see also Fig. 3*A*-*E*). Fig. 2*D* is from the same 3-D model, except that it is depicted with only unidirectional lighting. The 3-D model is based on segmentation of the two tomograms in the middle of the sequence shown in Suppl. 1. The video was created with Chimera.

Supplement 6. Video showing a double-tilt tomogram of the basal area of a mouse rod OS. As the video progresses through different z-planes, the number of nascent disks that are enclosed by the plasma membrane (right side) changes. The transition between 8 and 9 open disks can be observed 9-10 sec from the start of the video. Every second z-slice was exported from 3dmod as a tiff file and then converted into a video using Fiji. Images of

individual z-slices are shown in Fig. 3*F-H*, although note that the order of appearance in the video is *H*, *G* and then *F.*

Supplement 7. Video showing the 3-D model of a tomogram of a mouse rod OS. The video shows the plasma membrane modeled in green, the mature disks in dark blue. The plasma membrane of the distal inner segment and calycal process were modeled separately from the rest of the plasma membrane and are shown in light blue. Note that proximal to the area modeled and shown here, the plasma membrane surrounding the axoneme (i.e. the transition zone plasma membrane) will connect with the adjacent plasma membrane. The 3-D model rotates and then zooms in on the nascent disks, showing the close proximity of the outer and inner segment membrane structures. This 3-D model is based on segmentation of the tomogram shown in Suppl. 4, and the video has been made using Chimera. Images from this model are shown in Fig. 3*I* and *J*.

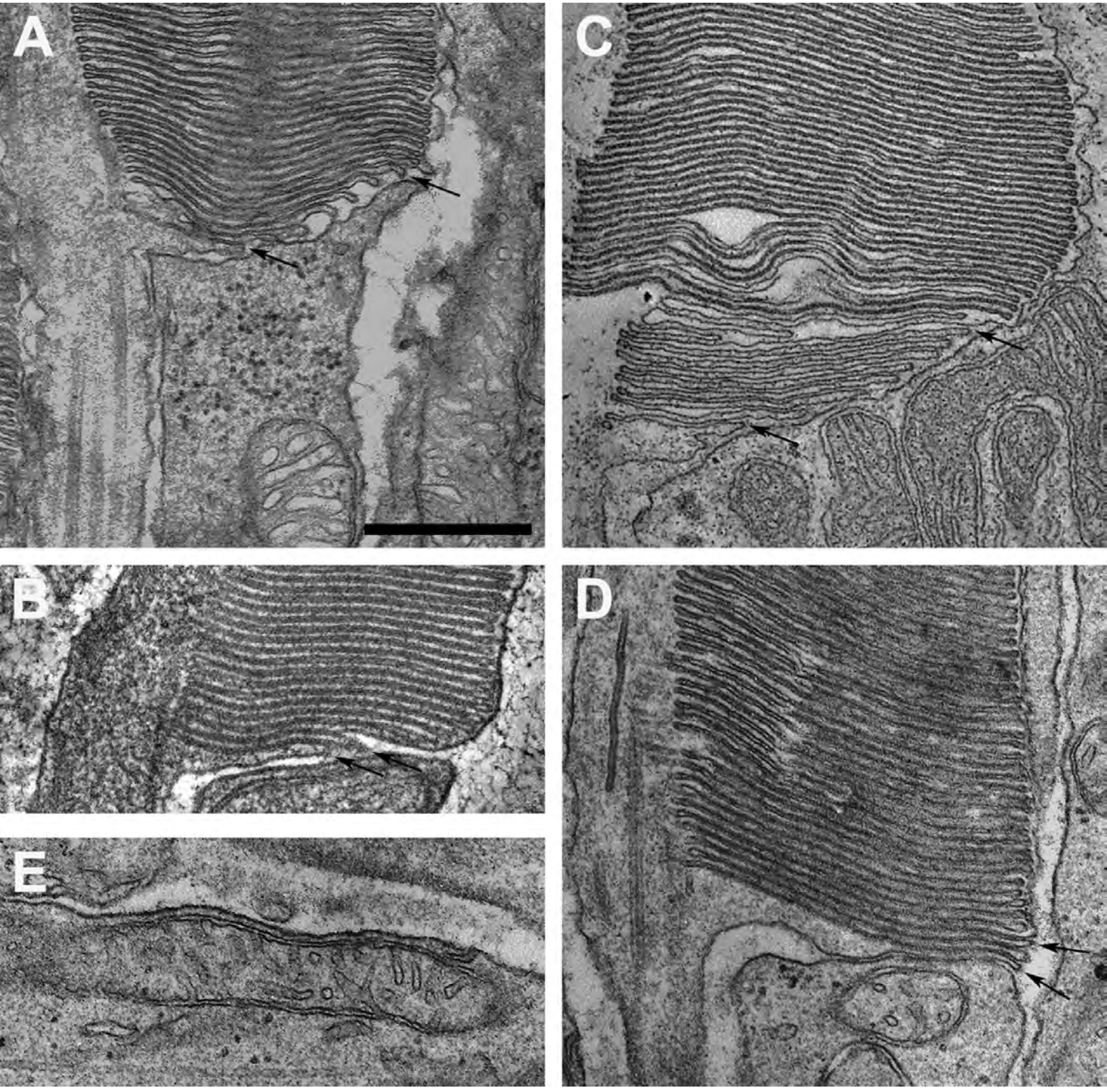
A
C
B
D
E

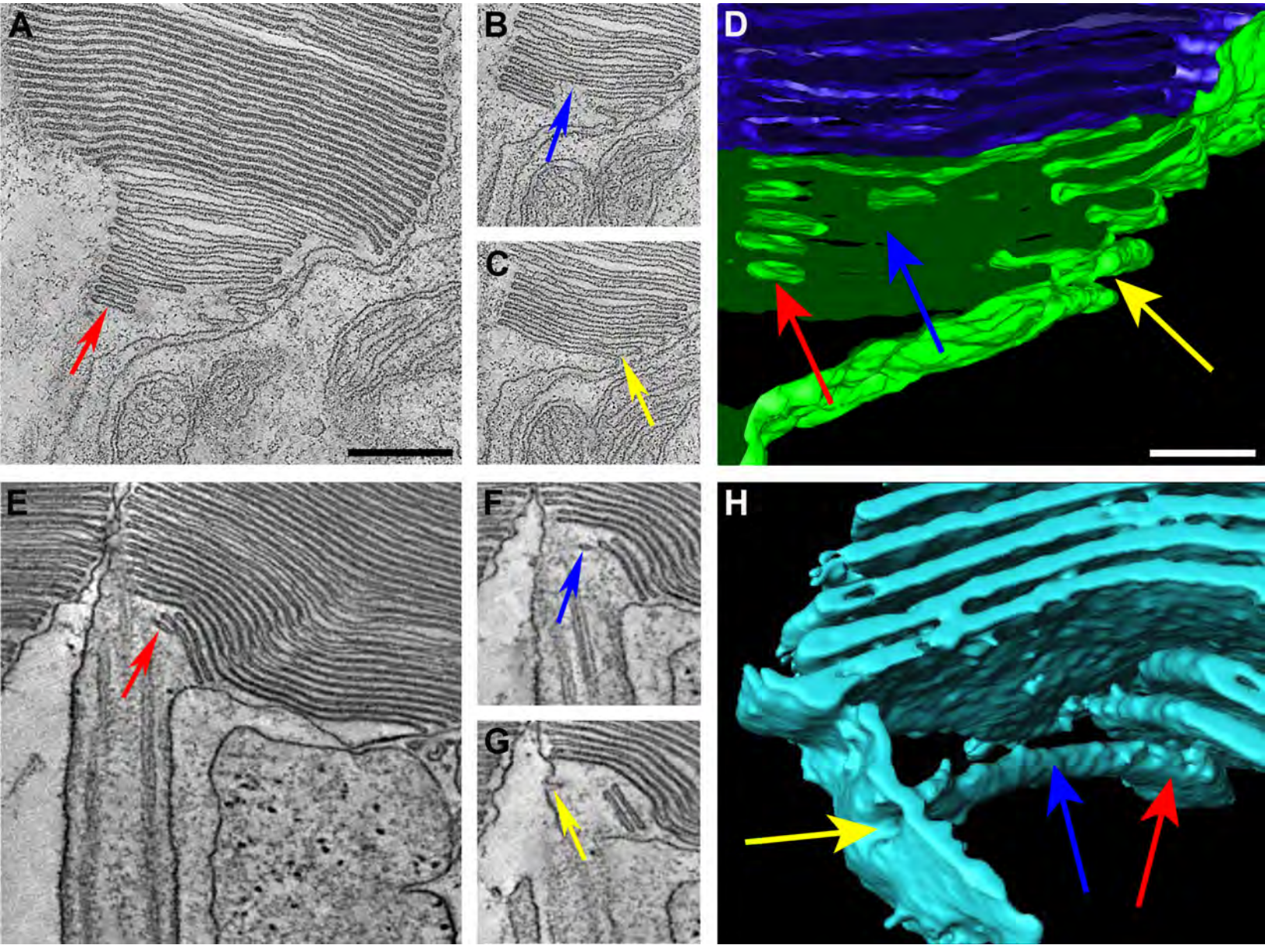
A
B
C
D
E
F
G
H

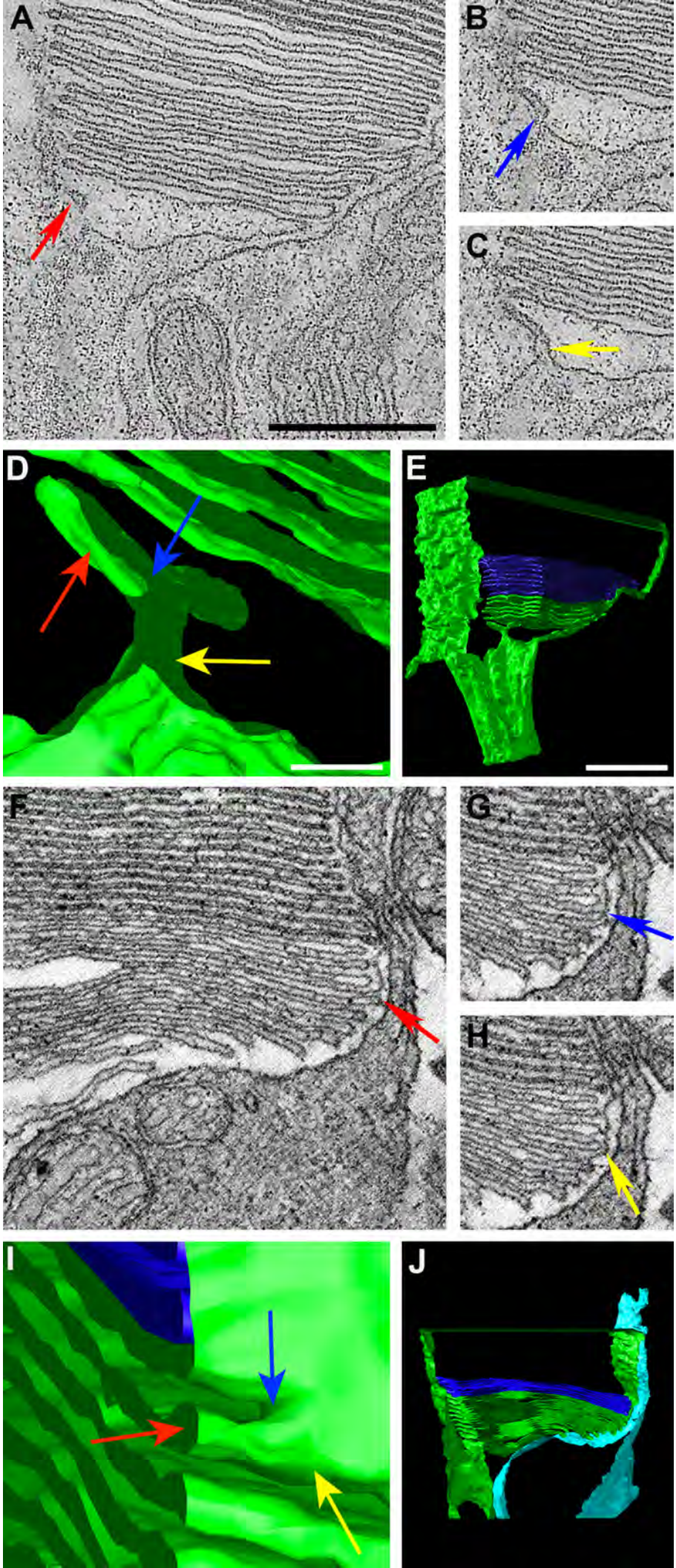
A
B
C
D
E
F
G
H
I
J

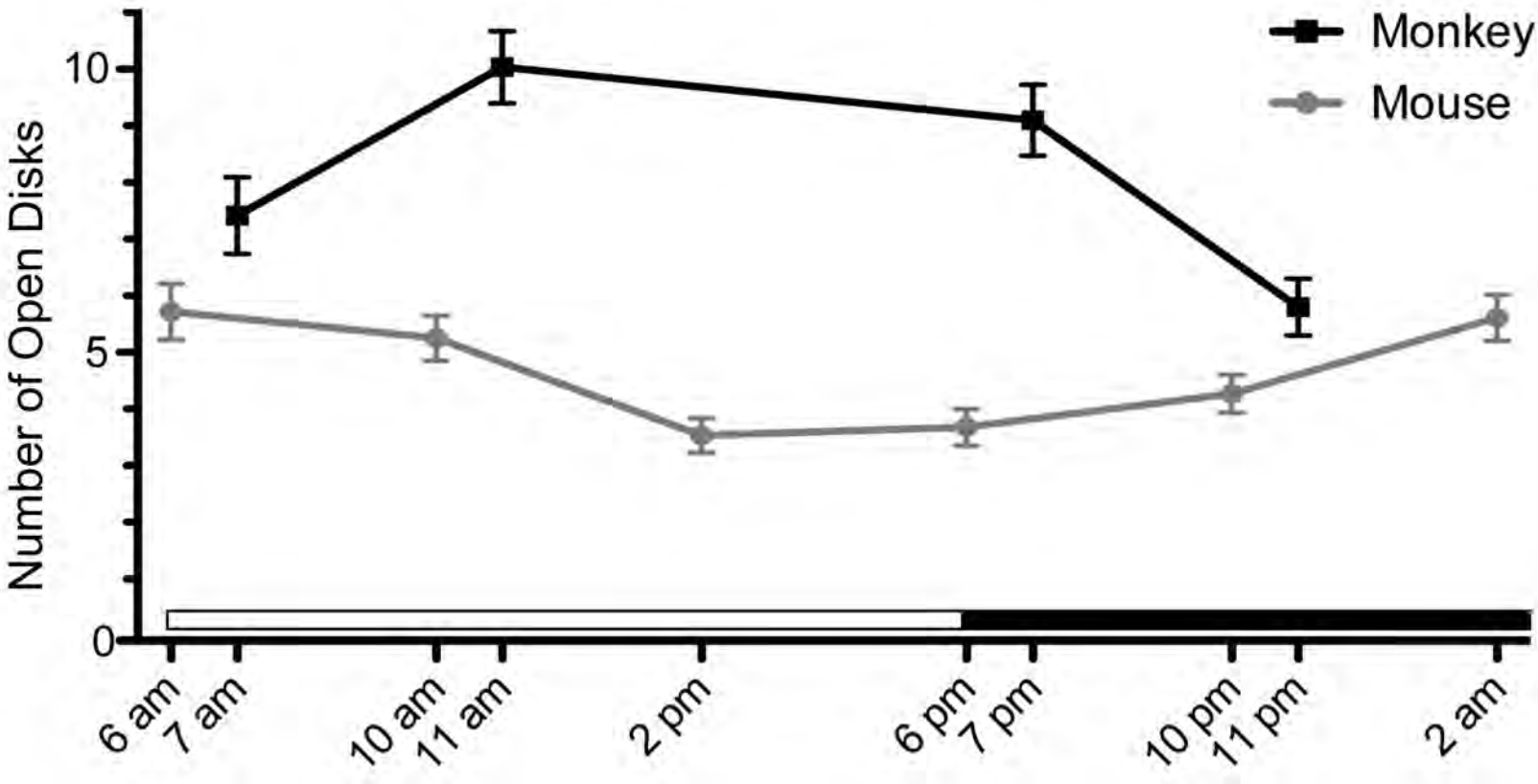
Monkey
Mouse
Number of Open Disks
10
5
0
6 am
7 am
10 am
11 am
2 pm
6 pm
7 pm
10 pm
11 pm
2 am

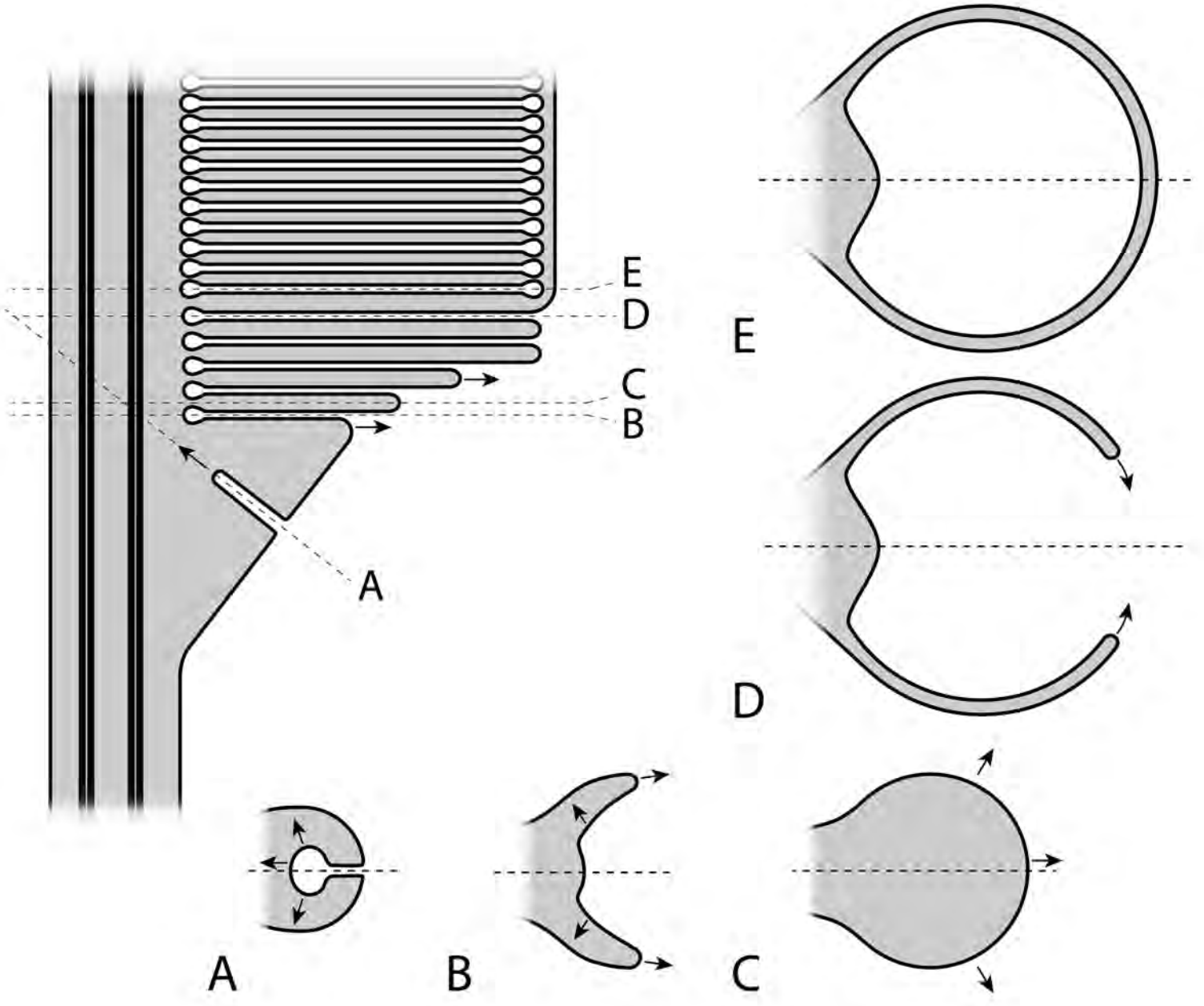
E
D
C
B
A
E
D
A
B
C